J. Fluid Mech. (1993), *vol.* 253, *pp.* 617–641

Flow of Newtonian and non-Newtonian fluids in concentric and eccentric annuli

By J. M. NOURI, H. UMUR AND J. H. WHITELAW

Imperial College of Science, Technology and Medicine, Mechanical Engineering Department, Thermofluids Section, Exhibition Road, London SW7 2BX, UK

(Received 28 February 1992 and in revised form 11 December 1992)

Three components of mean velocity and the corresponding Reynolds shear stresses have been measured in fully developed concentric and eccentric annulus flows of a Newtonian fluid at bulk-flow Reynolds numbers of 8900 and 26600 and a weakly elastic shear-thinning polymer at effective bulk-flow Reynolds numbers of 1150, 6200 and 9600. The diameter ratio was 0.5 with eccentricities of 0, 0.5 and 1.0, and the use of a Newtonian fluid of refractive index identical to that of the Perspex working section facilitated the measurements by laser velocimetry.

With the Newtonian fluid, the distribution of static pressure measurements on the outer wall is shown to be linear, with friction factors for concentric-annulus flows some 8% higher than in a smooth round pipe and for the eccentric flows of eccentricities of 0.5 and 1.0 it was lower by, respectively 8 and 22.5% than that of the concentric-annulus flow. In the former case, the law of the wall was confirmed on both inner and outer walls of the annulus at both Reynolds numbers. This was also the case for the outer wall in the eccentric-annulus flows, except in the smallest gap, but the near-inner-wall flow was not represented by a logarithmic region particularly in the smallest gap. The locations of zero shear stress and zero velocity gradient were displaced by amounts which were, like the secondary flows measured in the eccentric annulus of 0.5, almost within the measurement precision. In the eccentric-annulus flow with eccentricity of 1.0, there was a secondary flow with two circulation cells on each side of the plane of symmetry and with a maximum velocity of 2.2% of the bulk velocity.

The measurements with the non-Newtonian fluid were less detailed since refraction limited the flow accessible to the light beams. The average wall shear stress coefficient was similar to that for the Newtonian fluid in the laminar region of the concentric-annulus flow and higher for the two eccentric-annulus flows. Transition was extended to an effective Reynolds number well above that for the Newtonian fluid with a drag reduction of up to 63%. The near-outer-wall flows had logarithmic forms between the Newtonian curve and that of the maximum drag-reduction asymptote, and all fluctuation levels were less than those for the Newtonian fluid, particularly the radial and tangential components.

1. Introduction

Flows in annular passages are important in drilling wells where mud passes between the drill shaft and the well casing to remove cuttings and friction-generated heat. The fluids usually have non-Newtonian properties so that the variation of viscometric viscosity can be important together with velocity characteristics. The present investigation provides velocity information for the flow of a Newtonian fluid in concentric and eccentric annuli, at Reynolds numbers up to those of fully turbulent

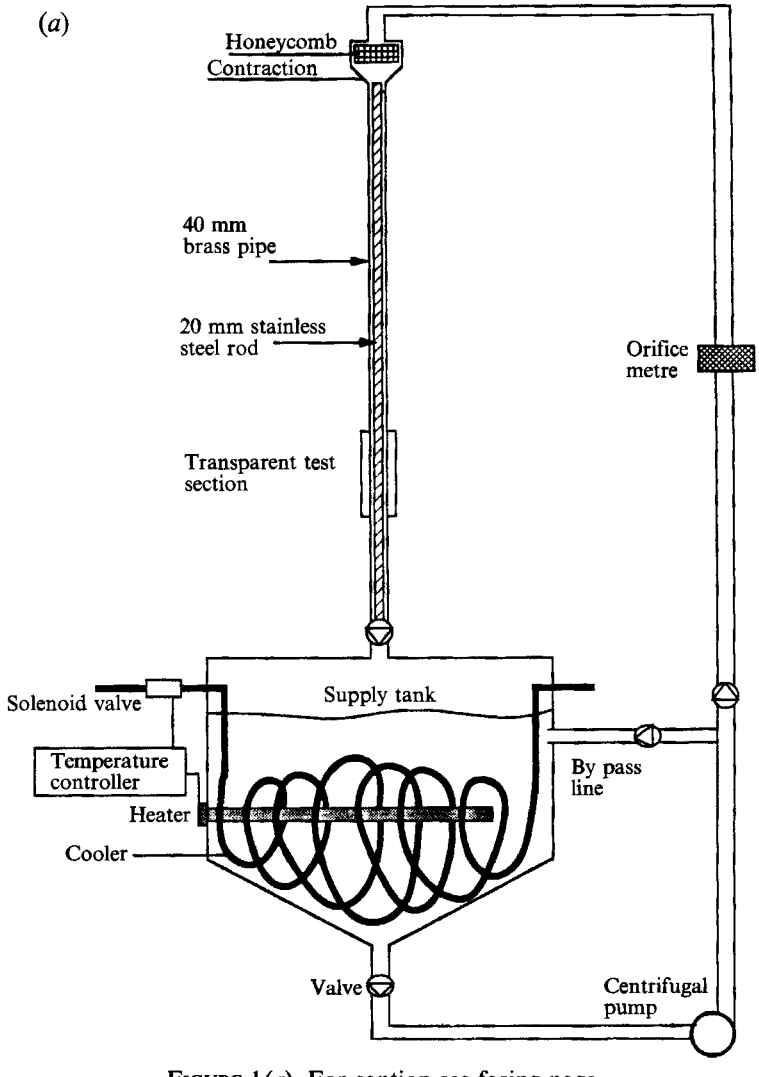

FIGURE 1(*a*). For caption see facing page.

flow, and a basis for comparison with corresponding results obtained in concentric and eccentric annuli with a non-Newtonian fluid.

The measurements of Pinho & Whitelaw (1990, 1991), the former in pipe flow, have shown that the general arrangement of the present flow is likely to lead to an effective Reynolds number, for a non-Newtonian fluid corresponding to a 0.2% aqueous solution of sodium carbomethyl cellulose (CMC), of the order of 9000 so that the present results include a Newtonian fluid flow with this Reynolds number. The viscometric properties of this fluid are known from Pinho & Whitelaw to be stable, appropriate to the drilling application and likely to lead to near-laminar friction factors approaching those of the maximum drag-reduction asymptote with suppression of turbulent fluctuations. The power-law viscometric form relating shear stress τ to shear rate γ,

$$\tau = 0.044\gamma^{0.75}, \tag{1}$$

is appropriate in the range of shear rates from 140 to 12000 s^{-1} and may be used in

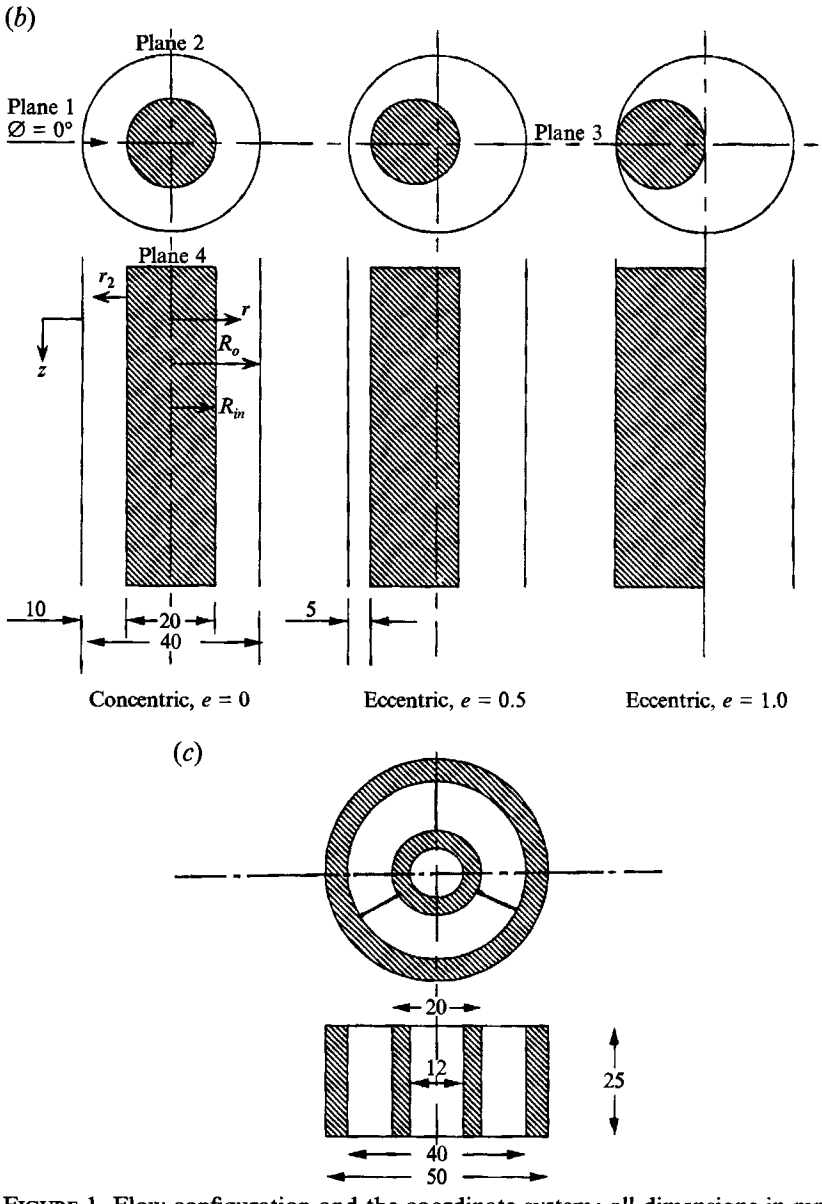

FIGURE 1. Flow configuration and the coordinate system; all dimensions in mm.

related calculations. It remains to be shown, however, how the fluid properties influence the flow in a non-concentric arrangement and this is a major purpose of the present investigation.

The Newtonian fluid was selected so as to allow the use of laser–Doppler velocimetry without limitations imposed by refraction. For this purpose, a mixture of 31.8% tetraline in turpentine was selected and maintained at a constant temperature of 25 ± 0.02°C. This selection of instrumentation and fluid allowed turbulent-flow Reynolds numbers to be achieved in a flow circuit and working section of modest dimensions with consequent cost saving and ease of manufacture to high tolerances. Further details on the use of refractive-index-matching techniques have been provided by Nouri, Whitelaw & Yianneskis (1988).

There have been many investigations of Newtonian fluid flows in concentric annuli and a few in eccentric annuli. The early work in the former has been reviewed by Rehme (1974) who referred to the well-known experiments of Brighton & Jones (1964) and Quarmby (1967). The controversy about the locations of velocity maximum and zero-shear stress, which can be important for calculations, was resolved by the investigations of Smith, Lawn & Hamlin (1968), Lawn & Elliot (1971) and Rehme who confirmed that the latter occurred closer to the inner wall. Shah & London (1978) showed analytically that the resistance to flow, for a Newtonian fluid, will be greatly affected in annulus flows: the flow resistance in the laminar region of a concentric annulus with a diameter ratio of 0.5, was 30% higher than that of the pipe flow and decreased with the eccentricity, and the flow resistance was some 36% lower than that of the pipe flow with eccentricity of unity.

Jonsson & Sparrow (1966) and Kacker (1973) examined eccentric-annulus turbulent flows and the results showed that the friction factor decreased with increasing eccentricity by up to 7% for an arrangement similar to that of the present study, that the near-wall flows deviated from the law of the wall, particularly at the inner wall where curvature can be important, and that a double-cellular structure existed with a maximum secondary-flow velocity of around 0.02 of the bulk flow velocity with a diameter ratio of 0.17 and an eccentricity of 0.47, defined by

$$e = \frac{l}{R_o - R_{in}} \tag{2}$$

with l the distance between the centres of the inner and outer pipes and R_{in} and R_o the inner and outer radii. The secondary flow feature is uncertain in view of the measurement difficulties associated with hot-wire instrumentation.

Previous measurements of non-Newtonian fluid flow in an annular passage are scarce, but there are many experimental investigations of the flows of non-Newtonian fluids in circular ducts, such as those of Park *et al.* (1989) and Pinho & Whitelaw (1990, 1991).

The present Newtonian fluid flows correspond to bulk-flow Reynolds numbers, based on bulk velocity, hydraulic diameter and fluid viscosity, of 8900 and 26600, in a concentric annulus with diameter ratio of 0.5 and, with the same rod and pipe, eccentricities of 0.5 and 1.0. The same flow circuit and concentric and eccentric-pipe arrangements were used with the non-Newtonian fluid, a 0.2% aqueous solution of CMC, leading to bulk velocities of 0.57, 1.99 and 2.76 m/s. There is no unique definition of Reynolds number for non-Newtonian fluid flow and here we prefer that based on bulk velocity, hydraulic diameter and viscosity at the wall which implies values of 1150, 6200 and 9600. The flow configuration and instrumentation are described briefly in the following section and the results presented and discussed in the third section. The paper ends with a summary of the more important findings.

2. Flow configuration and instrumentation

The flow arrangement is shown in figure 1 with the details of the test section and coordinate system in figure 1(*b*). A centrifugal pump delivered a mixture of tetraline and turpentine from a supply tank to a chamber where, after passing through a section of honeycomb and a contraction, it flowed into the annular passage with an outer brass pipe of nominal inside diameter, D_o, of 40.3 mm and 2.0 m long. An inner stainless steel rod of 20 mm diameter, D_{in}, was used to give a diameter ratio D_{in}/D_o of 0.5. The

	Concentric and eccentric flows	
Outer diameter, D_o (mm)	40.3	
Inner diameter, D_{in} (mm)	20.1	
Hydraulic diameter, $D_o - D_{in}$ (mm)	20.2	
Volume flow rate ($\times 10^{-3}$, m^3/s)	0.68	2.05
Bulk velocity, U_b (m/s)	0.72	2.15
Reynolds number, Re ($\times 10^3$)	8.9	26.6
Fluid mixture temperature (°C)	25.0 ± 0.02	
Density of the mixture, ρ (kg/m^3)	896.0	
Kinematic viscosity of the mixture, ν ($\times 10^{-6}$ m^2/s)	1.63	
Refractive index of the mixture at $\lambda = 589.6$ nm	1.489	

TABLE 1. Newtonian fluid flow properties and properties of mixture of 31.8% tetraline in turpentine

bulk flow rate was measured by a calibrated orifice plate with precision better than 3% for Newtonian fluid flow, but with 0.2% CMC the reading from the orifice plate underestimated the values of bulk velocities by 16% when compared with those obtained from integration of mean velocity profiles, and this was corrected accordingly. The temperature of the mixture and the CMC was controlled to 25.0 ± 0.02 °C so that in the case of mixture flow the refractive index was 1.489, identical to that of the Plexiglas material used to form the test section.

To ensure fully developed flow in the measuring section, the length of the straight pipe upstream of the test section was 2.32 m, corresponding to 116 hydraulic diameters or 58 outer-pipe diameters, with a uniform step at the inlet in order to produce an artificially thickened boundary layer.

The outer diameter of the test section was machined from a rectangular block of Plexiglas and the inner shaft from a Plexiglas rod. Both were carefully annealed at 85 °C for 25 h with slow heating and cooling rates to avoid chemical attack. The outer rectangular shape avoided asymmetric refraction of the light beams at the outer wall. The rectangular test section was connected to brass pipes and the inner Plexiglas shaft to stainless steel rods. The inner rod was positioned in the outer pipe with four brass spiders close to the inlet of the brass pipe, $5D_o$ upstream of the test section, and a further two downstream of the test section. In the eccentric-annulus flow configurations, the distance, l, between the centre of the inner shaft and the outer pipe was 5 and 10 mm which gave eccentricities of 0.5 and 1.0. A typical spider is shown in figure 1(*c*) for the concentric geometry, with the three legs streamlined and with a maximum thickness of 1.5 mm. The bulk flow conditions and properties of the Newtonian and non-Newtonian fluids are given in tables 1 and 2.

The dynamic viscosities listed in table 2 and used in the effective Reynolds number were obtained by dividing the average wall shear stress, determined from pressure measurements, by the shear rate determined from the power-law relationship for 0.2% CMC (equation (1)). Similar rheological measurements to those of Pinho & Whitelaw (1990) were carried out with 0.2% CMC solutions and the viscosity results were all within 5%. These results also confirmed that the 0.2% CMC degraded by less than 10% after 6 h of operation in the present flow configuration.

Static pressures were measured with holes of 0.5 mm diameter distributed longitudinally and circumferentially around the outer diameter. The static pressures were read from a calibrated manometer bank with ± 1 mm resolution. The specific

	Concentric and eccentric flows		
Outer diameter, D_o (mm)		40.3	
Inner diameter, D_{in} (mm)		20.1	
Hydraulic diameter, $D_o - D_{in}$ (mm)		20.2	
Volume flow rate ($\times 10^{-3}$, m^3/s)	0.541	1.90	2.646
Bulk velocity, U_b (m/s)	0.565	1.986	2.757
Viscosity at wall, μ_w ($\times 10^{-3}$ kg/m s)	9.75	6.4	5.7
Reynolds number, Re ($\times 10^3$)	1.15	6.2	9.6
CMC temperature (°C)		25.0 ± 0.02	
Density of the CMC, ρ (kg/m^3)		1000.0	
Refractive index of CMC at λ = 589.6 nm		1.33	

TABLE 2. Non-Newtonian fluid flow properties and properties of 0.2% aqueous solution of CMC

Focal length of the focusing lens (mm)	200.0	300.0
Half angle of the beam interaction (degrees)	8.92	5.98
Fringe spacing (μm)	2.04	3.04
Number of fringes without frequency shift	20	20
Diameter of the control volume at $1/e^2$ intensity in air (μm)	41.0	61.0
Length of the control volume at $1/e^2$ intensity in air (μm)	260.0	580.0
Maximum frequency shift (MHz)	±3.0	±3.0
Frequency to velocity conversion (ms^{-1}/MHz)	2.04	3.04

TABLE 3. Characteristics of optical arrangement

gravity of the manometer fluid was 1.88 with a height range of 20–400 mm. The maximum uncertainties were less than ±5 and ±2.5% for the turbulent flow of the Newtonian fluid and polymer solution respectively. Pressure measurements for Newtonian laminar and transitional regions were carried out using an aqueous solution of glycerol with kinematic viscosity of 9.52 mm^2/s and density of 1140 kg/m^3.

The laser–Doppler velocimeter was identical to that described by Nouri & Whitelaw (1991) and comprised a 5 mW helium–neon laser, a diffraction-grating unit to divide the light beam and provide frequency shift, a focusing lens to form the control volume in the test section, a lens located on the axis to collect forward-scattered light, a pin hole and a photomultiplier. The principal characteristics of the optical system are given in table 3. The signal from the photomultiplier was processed by a frequency counter interfaced to a microprocessor and led to ensemble-averaged values of mean and r.m.s. velocities. The Reynolds shear stresses were obtained as by Melling & Whitelaw (1976) from the r.m.s. velocity measurements in the planes at ±45° to the main flow.

With the water-based liquids (0.2% CMC and glycerol), the velocity gradient was aligned across the length of the measuring volume and particular care was taken close to the solid boundary by reducing the power supply of the photomultiplier and off-axis collection of the scattered light to ensure that the Doppler bursts stemmed from the central region of the measuring volume. The resulting velocity gradient were significant for Y^+ less than around 20, and corrections were applied according to the method described by Durst, Melling & Whitelaw (1981). The maximum uncertainties in mean and r.m.s. velocities close to a solid boundary were 2.5% and 6% respectively.

With the refractive-index-matched fluid the measuring volume was aligned so that the velocity gradient was across its smaller dimension and no corrections for velocity

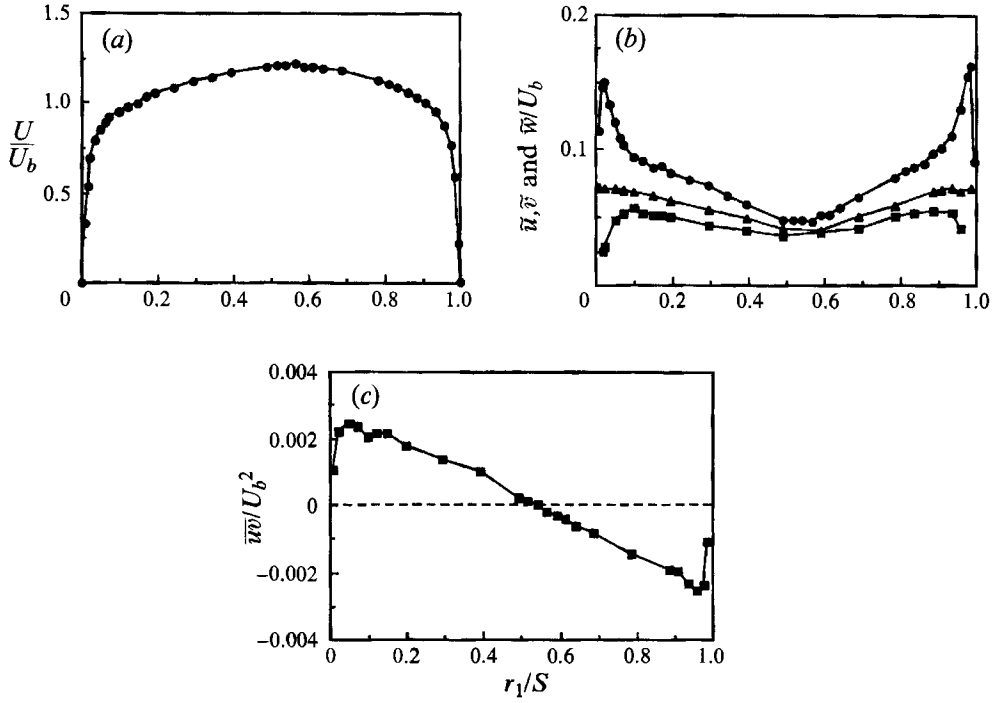

FIGURE 2. Newtonian fluid in a concentric annulus with Reynolds number of 26600: (*a*) axial mean velocity; (*b*) r.m.s. of velocity fluctuations: —●—, axial; —■—, radial; —▲—, tangential; (*c*) $\overline{uv}$ cross-correlation.

gradient were necessary; the maximum uncertainties in gradient broadening close to the wall (i.e. 0.1 mm from the wall) were calculated to be 0.2 and 1.6% of the local values of the axial mean and r.m.s. velocities respectively. For the tangential velocity and $\overline{uw}$ cross-correlation, the length of the measuring volume was parallel to the velocity gradient and, although the tangential velocity was unaffected since there was no velocity gradient, the $\overline{uw}$ cross-correlation was affected by the spatial variations of mean velocity. However, corrections were uncertain since $\overline{uw}$ was obtained from measurements in planes at $\pm 45°$ to the main flow; the uncorrected results had values of $\overline{uw}$ up to $0.001 U_b^2$ close to the inner and outer walls (up to 1 mm from the walls) and zero over the central region.

Systematic positional errors up to half of the length or diameter of the measuring volume were possible and were avoided by careful examination of the near-wall measurements. With the mixture flow, the measuring volume was easily positioned so as to touch the outer wall and a correction of half the diameter of the measuring volume was applied to radial distance. With the 0.2% CMC solution, the centre of the length of the measuring volume was positioned on the outer wall with a magnifying lens and, by comparing the results of Y^+ in the wall-law coordinates, it was found that the values of Y^+ were shifted towards the wall by one quarter of the nominal length of the measuring volume and a correction was made for this distance: the effect was examined with concentric and eccentric arrangements and was found to be the same. It should be emphasized that the related uncertainties had no influence on the logarithmic region nor on the conclusions drawn from the investigation. More than 3000 samples were collected for all measurements to minimize the statistical error and this was increased to 4000 for the cross-correlations.

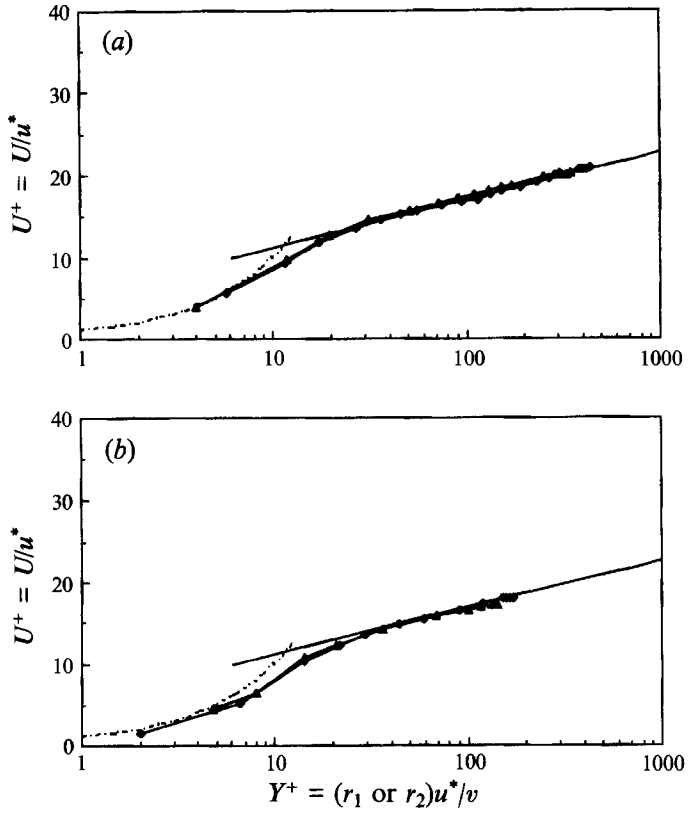

FIGURE 3. Axial mean velocity profiles in law-of the-wall coordinates; Newtonian fluid in a concentric annulus: (*a*) $Re = 26600$; (*b*) $Re = 8900$: —◆—, outer-wall profile; —▲—, inner-wall profile; ——, Clauser, $U^+ = 2.44 \ln Y^+ + 4.9$; –·–·–·–, $U^+ = Y^+$.

In their investigation of the fully-developed flow in a square duct, Melling & Whitelaw (1976) quantified the uncertainties associated with secondary flows as of the order of 0.015 of the bulk-flow velocity with laser-velocimeter signals and fringes aligned $\pm 45°$ to the main flow. They concluded that the uncertainties in secondary velocity could exceed 0.009 of the bulk-flow velocity and preliminary investigations in the present flow showed a similar result, so that this technique did not allow a definite conclusion about the existence of secondary flows. The use of frequency shift can, in principle, allow the direct measurement of secondary flow velocities and a Bragg cell was used for this purpose since it ensured sufficient fringes even with the low secondary-flow velocities and large angle to the bulk flow. Uncertainties were estimated to be 0.006 of the bulk-low velocity, which is an improvement on that of Melling & Whitelaw. Nevertheless, the secondary-flow velocities are subject to uncertainties of up to 40% of the maximum measured value.

3. Results and discussion

Velocity results are presented separately for the concentric and eccentric flows and have been normalized with bulk velocities, U_b, and maximum velocities, U_m. Distances are normalized with the radial distance S from the outer to inner wall, which is constant at 10.15 mm for the concentric arrangement and varied from 5.3 to 20 mm for the eccentric arrangements.

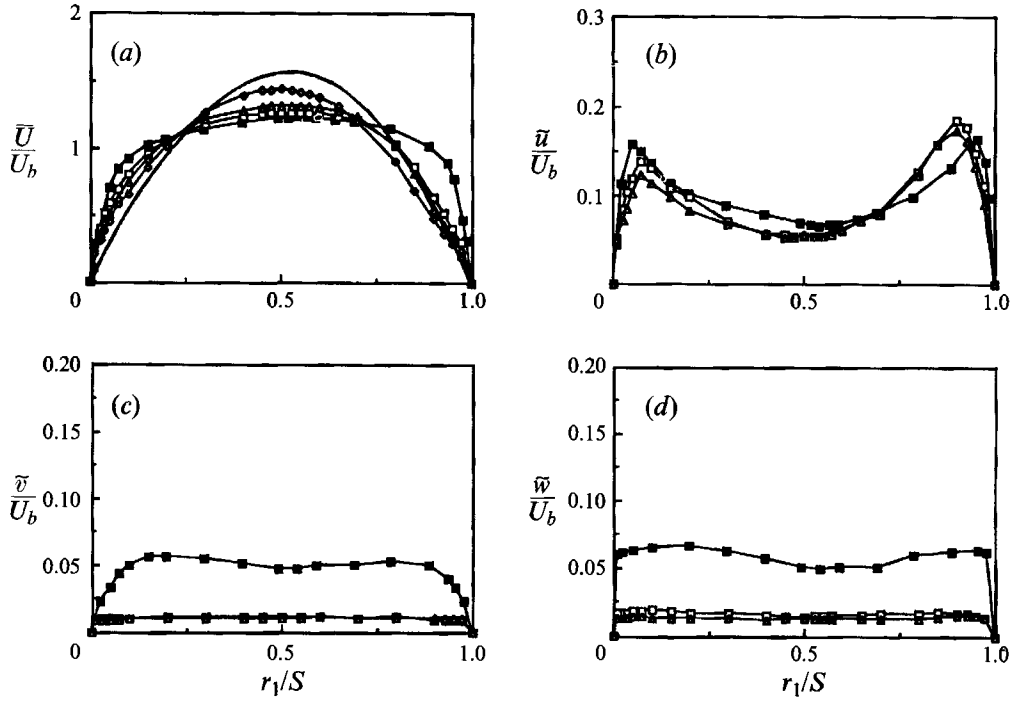

FIGURE 4. Non-Newtonian fluid in a concentric annulus for three effective Reynolds numbers: (*a*) axial mean velocity; (*b*) axial r.m.s. velocity; (*c*) radial r.m.s. velocity; (*d*) tangential r.m.s. velocity: —■—, Re = 8900, Newtonian; —□—, 9600, CMC; —△—, 6200, CMC; —◇—, 1150, CMC; ——, Newtonian theoretical laminar mean velocity profile.

3.1. *Concentric arrangement*

Profiles of axial velocity and the Reynolds stresses were measured for the two Reynolds numbers after it had been confirmed that the flow was fully developed and symmetrical. This confirmation involved the measurement of the axial pressure gradient which was found to be constant with the axial distance. Mean velocity profiles measured on four quadrants and at locations separated by a distance of 5 hydraulic diameters were identical within the measurement uncertainty of $0.01U_b$ and led to integrated, bulk velocities within 1% of each other. Thus the results of figure 2 correspond to a symmetrical and fully developed flow with a Reynolds number of 26600 and show the expected velocity maximum of $1.22U_b$, located towards the inner wall and at a location displaced by $0.02S$ from the location of zero $\overline{uv}/U_b^2$. No cross-stream velocities were detected and the fluctuation velocities behaved as expected with magnitudes decreasing from axial, to circumferential, to radial components. The shear stress coefficient, $\overline{uv}/U_b^2$, has an extensive linear region with maxima of 2.41×10^{-3} and 2.53×10^{-3} close to outer and inner walls respectively.

The results at the lower Reynolds number are similar to those of figure 2 with a maximum normalized velocity 2% higher than that at the higher Reynolds number. The fluctuation velocities were also similar and the locations of zero shear stress were again close to that of the velocity maximum. Further details of these results are presented below where they are compared with those obtained with the non-Newtonian fluid.

The wall shear stress at the inner and outer walls with the Newtonian fluid can be

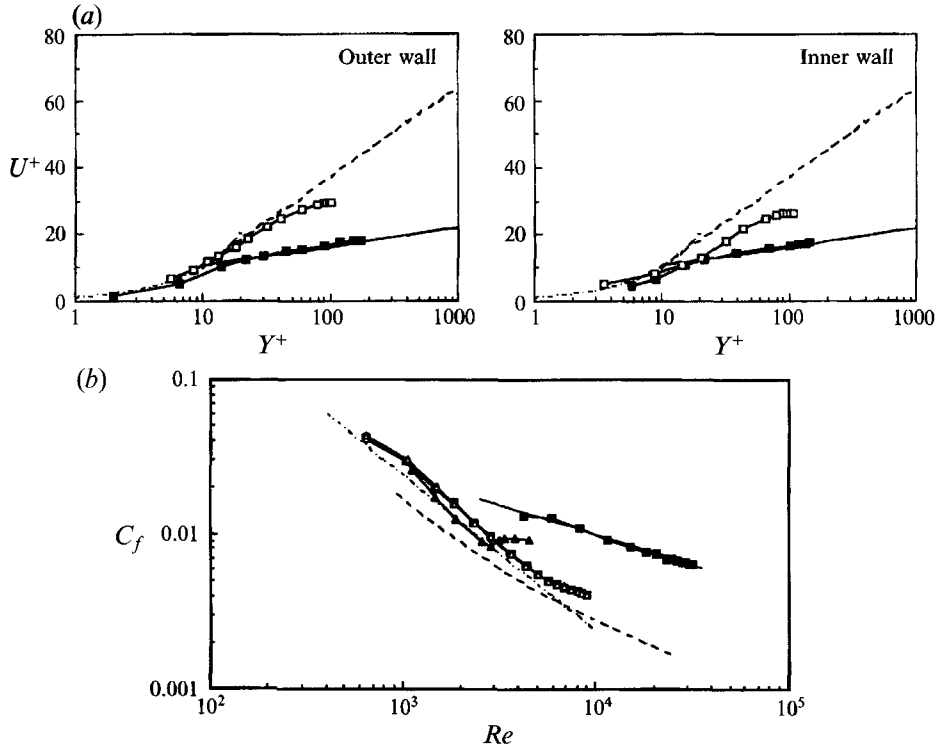

FIGURE 5. Non-Newtonian fluid in a concentric annulus: (*a*) axial mean velocity profiles in law-of-the-wall coordinates for an effective Reynolds number of 9600, symbols the same as in figure 4, ——, $U^+ = 2.44 \ln Y^+ + 4.9$; ——, $U^+ = 11.7 \ln Y^+ - 17$; ————, $U^+ = Y^+$; (*b*) skin-friction coefficient as a function of Reynolds number: —▲—, --■--, Newtonian concentric for laminar and turbulent regions; —⊡—, CMC, plane 1; —○—, CMC, plane 2; —△—, CMC, plane 3; —◇—, CMC, plane 4; ——, $C_f = 0.36Re^{-0.39}$; ——, $C_f = 23.8Re^{-1}$; ——, maximum drag-reduction asymptote.

calculated from pressure measurements and the zero-shear-stress location with the equations

$$\tau_o = -\left(\frac{\partial P}{\partial z}\right)\left[\frac{R_o^2 - R_m^2}{2R_o}\right], \tag{3}$$

$$\tau_{in} = -\left(\frac{\partial P}{\partial z}\right)\left[\frac{R_m^2 - R_{in}^2}{2R_{in}}\right] \tag{4}$$

obtained from the momentum equation for fully developed, axisymmetric, steady and incompressible flow, where τ_o and τ_{in} are the outer and inner wall shear stresses and R_m is the location of zero shear stress. Since the location of the maximum mean velocity could not be distinguished from that of the zero shear stress and, consistent with the calculation of the wall shear stresses with the non-Newtonian fluid in which the shear stress could not be measured here, we preferred to use R_m as the radius of the maximum mean velocity. This gave values of τ_{in} and τ_o at the higher Reynolds number of 14.86 and 14.05 Pa respectively with a ratio of 1.06; this corresponds to a location of maximum mean velocity of $r_1/S = 0.572$ in figure 2(*a*). The corresponding values at the lower Reynolds number were 2.42 and 2.18 Pa with a ratio of 1.1. Figure 3 shows the near-wall velocity profiles in wall-law coordinates with r_1 and r_2 the distances from the outer and inner walls respectively. It is evident that the two

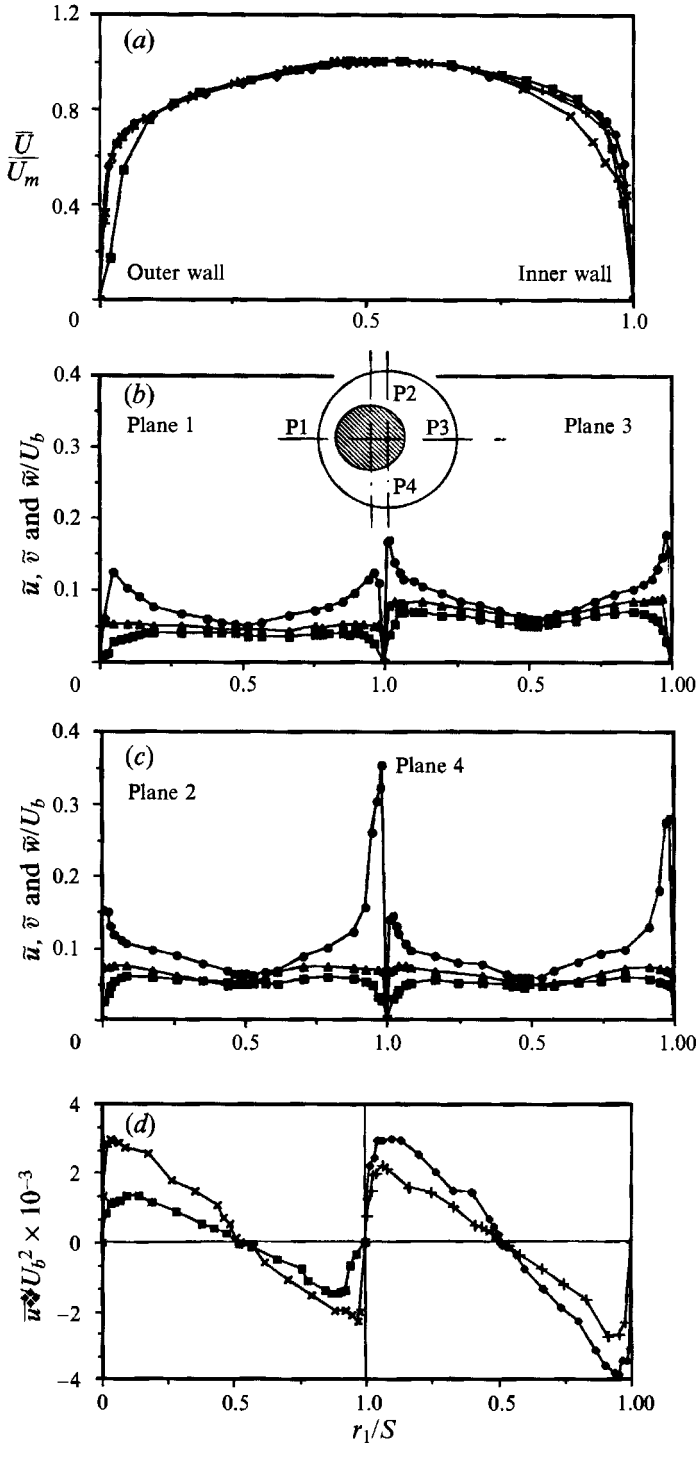

FIGURE 6. Newtonian fluid in an eccentric annulus with $e = 0.5$ for a Reynolds number of 26600: (*a*) axial mean velocity: —■—, plane 1; —×—, plane 2; —◆—, plane 3; —+—, plane 4. (*b*, *c*) r.m.s. velocity fluctuations, symbols the same as in figure 2(*b*); (*d*) $\overline{uv}$ cross-correlation, for symbols see (*a*).

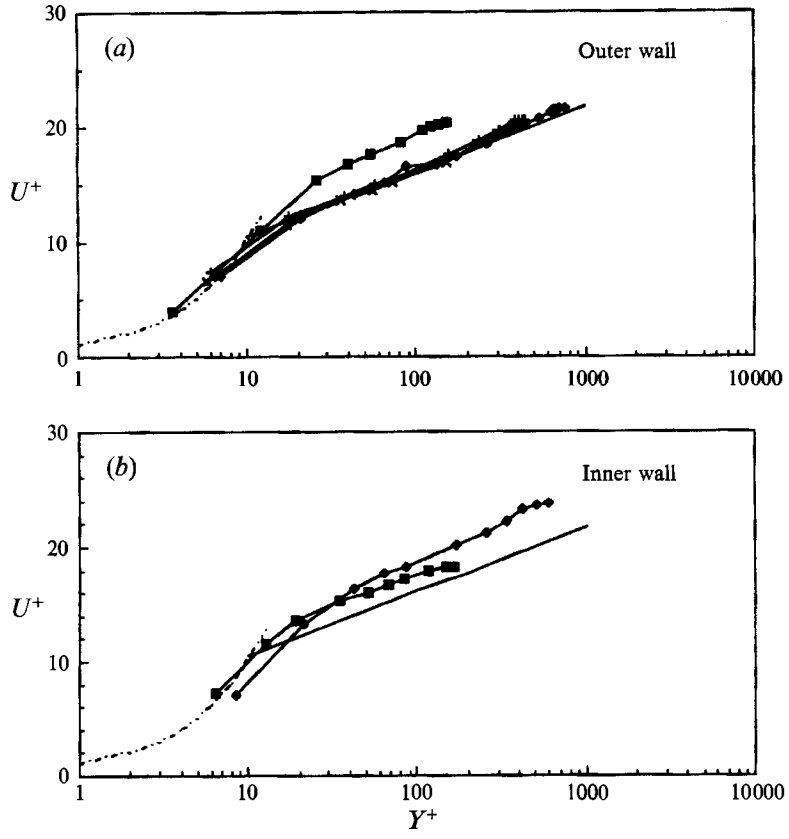

FIGURE 7. Axial mean velocity profiles in law-of-the-wall coordinates: Newtonian fluid in eccentric annulus with $e = 0.5$ for a Reynolds number of 26600: (*a*) outer wall; (*b*) inner wall. ——, $U^+ = 2.44 \ln Y^+ + 4.9$; – – – – –, $U^+ = Y^+$. For symbols see figure 6(*a*).

Reynolds numbers lead to near-wall profiles which possess a logarithmic region similar to that of the accepted law of the wall.

The overall skin-friction coefficient was obtained from pressure measurements as

$$C_f = \left(\frac{\partial P}{\partial z}\right)\left[\frac{d_h}{2\rho U_b^2}\right], \tag{5}$$

and a least square fit led to the expression

$$C_f = 0.36\,(Re)^{-0.39} \tag{6}$$

for Reynolds numbers from 4000 to 30000. The measurements are up to 8% larger than those for smooth circular pipe and some 2% greater than the Newtonian pipe flow results of Pinho & Whitelaw (1990). This is in accord with previous findings which showed that frictional losses in concentric annuli are some 3–10% higher than in smooth pipe flow.

The results obtained with the Newtonian fluid at a Reynolds number of 8900 and with the 0.2% solution of CMC at three effective Reynolds numbers are presented on figures 4 and 5. The Newtonian-fluid mean velocities of figure 4(*a*) are almost identical to those of figure 2(*a*) for the higher Reynolds number. The non-Newtonian fluid, normalized with its higher bulk velocity, has a near-wall form closer to that expected

with a laminar boundary layer and this is emphasized as the effective Reynolds number is decreased. In comparison to the Newtonian laminar mean velocity profile from Shah & London (1978), the CMC profile at the Reynolds number of 1150 shows a flatter and less skewed profile with a normalized maximum velocity 8.5% lower due to the shear-thinning effect. The maximum velocities of 0.2% CMC are at the middle of gap with values of 1.45, 1.33 and 1.27 times the bulk velocities for effective Reynolds numbers of 1150, 6200 and 9600 respectively. The turbulence intensities for the Newtonian fluid, figure 4(*b–d*), are also similar to those of figure 2(*b*) and decrease appreciably for the non-Newtonian fluid, particularly for the radial and tangential components which are smaller by a factor of 3.5. This behaviour of the fluctuation velocities is consistent with that of Pinho & Whitelaw (1990) and suggests that the differences between the Newtonian and non-Newtonian fluids are greater than those due to the effective Reynolds number. The differences are associated with the preferential orientation of the polymer molecules and the increased resistance of stretched molecules to deformation.

The near-wall velocities for the non-Newtonian fluid flows do not obey the law of the wall, as shown in figure 5 (*a*), though they may be said to have a short logarithmic region which conforms to an expression which is different for the inner and outer walls. The values of U^+ and Y^+ for the non-Newtonian fluid flows are based upon the average shear stresses, calculated from (3) and (4) and assuming that the locations of zero shear stress and maximum mean velocity are the same as for the lower Reynolds number of Newtonian fluid flow. The higher values of U^+ for the 0.2% CMC flows are clear evidence of drag reduction. The variation of the average skin-friction coefficient with Reynolds number is shown on figure 5(*b*) together with the Newtonian laminar curve for concentric flow ($C_f = 23.8Re^{-1}$, from Shah & London) and the maximum drag reduction asymptote of Virk, Mickley & Smith (1970). The results for the Newtonian fluid in the turbulent region correspond to (6), and in the laminar region they agree well with the analytical solution and show that transition takes place at a Reynolds number of around 2500. The non-Newtonian fluid has an extended range of non-turbulent flow with values of C_f some 5% higher than those of laminar flow and up to 15% higher than that of the maximum drag reduction asymptote with drag reduction of 63% (defined as $d_r = 100[(C_{f_n} - C_{f_p})/C_{f_n}]$ where suffixes n and p represent the skin-friction coefficient for Newtonian and non-Newtonian fluids) at the same Reynolds number of 9600. This is consistent with the shape of the profile of figure 4(*a*) and with the reduction in the values of turbulence intensity but is higher by about 4% than the values determined by Pinho & Whitelaw in their pipe flow for the same CMC solution and at the same effective Reynolds number of 9600.

3.2. *Eccentric arrangements*

Measurements similar to those of §3.1 were obtained with eccentricities of 0.5 and 1.0 and, because the results differ from one radial plane to another, require more figures to present. The results for the eccentricities of 0.5 and 1.0 will be presented and discussed separately.

3.2.1. *Eccentricity of* 0.5

Again a high-Reynolds-number Newtonian fluid flow was investigated with the results shown in figures 6–8. The variation in the mean-velocity profiles, figure 6(*a*), is considerable with the maximum velocities in quadrants 1–4 corresponding to 0.85, 1.21, 1.41 and 1.18 of the bulk velocity, giving a maximum difference of 40% between

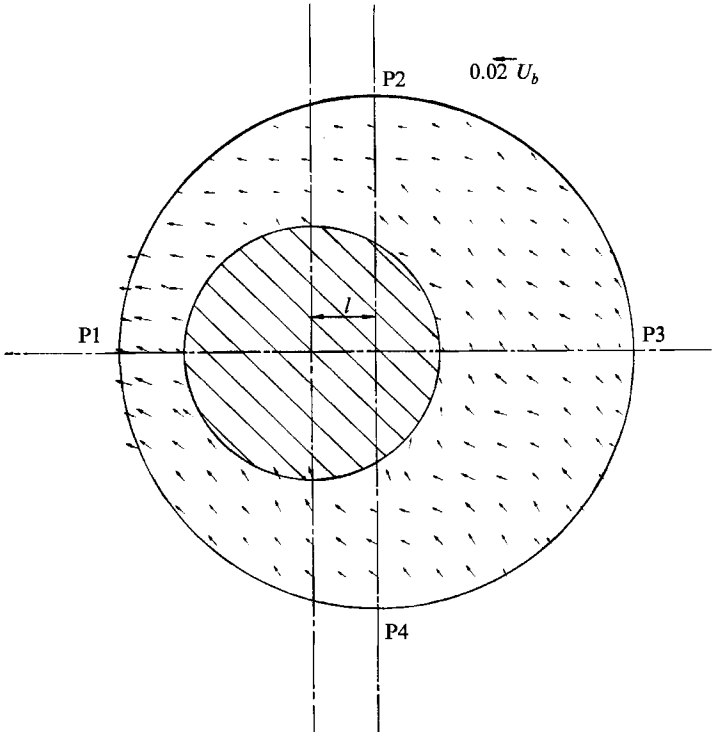

FIGURE 8. Vector velocity distribution of the cross-flow for a Reynolds number of 26600: Newtonian fluid in an eccentric annulus with $e = 0.5$.

the narrowest and largest gaps. The difference in maximum velocities in the symmetrical planes 2 and 4 is 3%, almost within the measurement accuracy, and probably due to a small asymmetry in the geometry. As will be shown later, the circumferential variation of axial velocity is also dependent on bulk Reynolds number and is different for the non-Newtonian fluid, which suggests that non-dimensionalization with the maximum velocity at each plane is more appropriate than use of the bulk velocity. The maximum velocities occurred at locations indistinguishable from the gap centre except in plane 3 where it was closer to the inner wall, at r_1/S of 0.55. The turbulence intensities and shear stresses, figures 6(*b*, *c*) and 6(*d*), also vary with circumferential location so that the turbulence intensities are smallest in the narrowest gap, that is plane 1. The maximum shear stress in plane 1 is also lower by a factor of 2.9 compared with the maximum value which occurs in plane 3. In all cases, the profiles of shear stress become zero at locations which correspond to the middle of the gap within measurement precision.

The mean velocities in the near-wall region are presented in wall-law coordinates in figure 7 and those at the outer wall accord closely with the law of the wall except in the narrowest gap where the higher values suggest a flow which is not fully turbulent. At the inner wall, velocities are presented for planes 1 and 3 and show that the inner pipe curvature has influenced the flow so that, again, the results are higher than those of the law of the wall and in accord with the findings of Sparrow, Eckert & Minkowycz (1963), Jonsson & Sparrow (1966) and Kacker (1973). The friction factors are some 8% smaller than those obtained with the concentric annulus.

It is evident from the findings of Jonsson & Sparrow and Kacker that secondary flows, driven by the normal stresses, can exist in non-circular ducts, but they should be

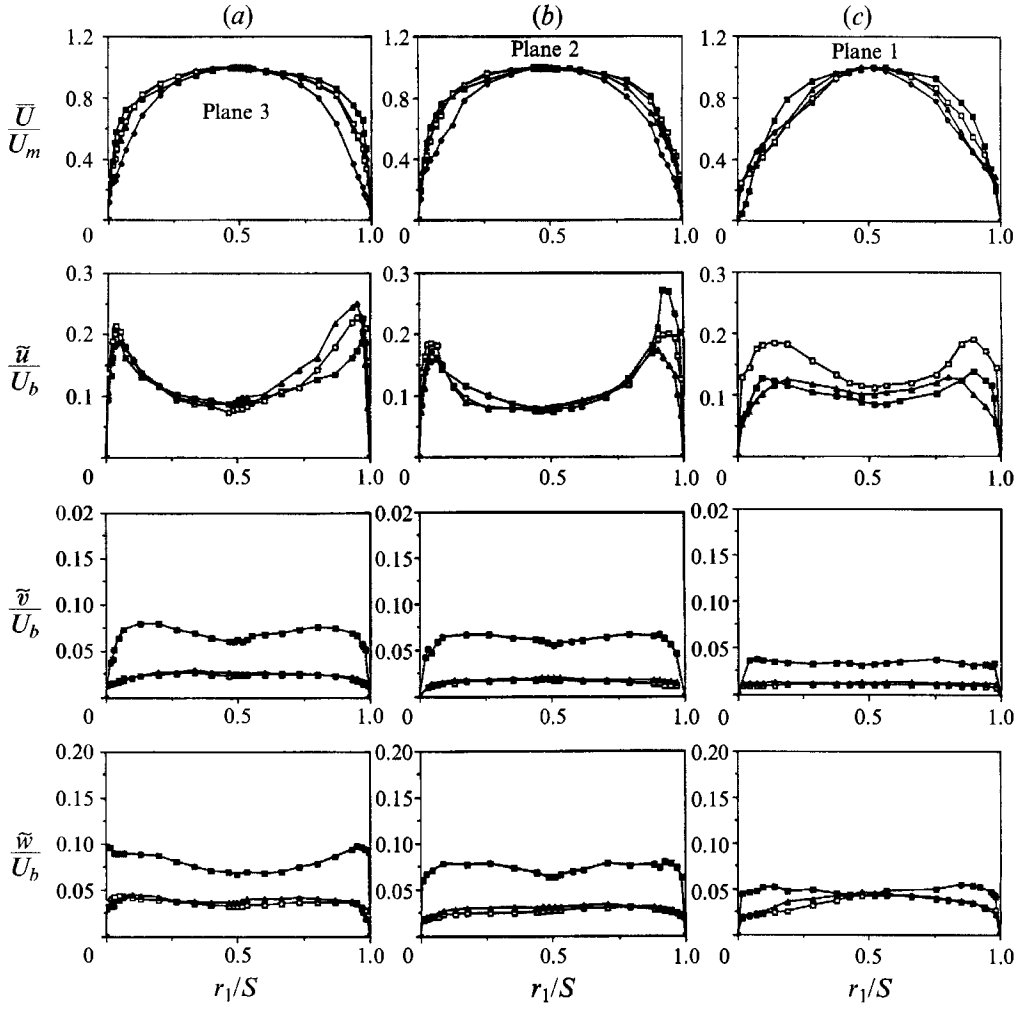

FIGURE 9. Mean and r.m.s. velocities of non-Newtonian fluid in eccentric annulus with $e = 0.5$ for three effective Reynolds numbers: (*a*) plane 3; (*b*) plane 2; (*c*) plane 1. For symbols see figure 4.

small with the present combination of radii and eccentricity. Figure 8 shows secondary-flow vectors measured here with the Bragg-cell method indicated in the introduction and with uncertainties of the order of 40% of the largest velocity shown on figure 7. The results must be considered with the caution but it appears that there is a small secondary flow generally from the wider gaps towards the narrowest gap or towards the bulk-flow direction.

Measurements of velocity and wall-pressure characteristics were also obtained at a Reynolds number of 8900 and are used in the following figures to compare with results obtained with the non-Newtonian fluid at three effective Reynolds numbers. One feature of note is that the difference between the maximum velocities at planes 1 and 3 was 10% larger than at the higher Reynolds number.

Figure 9 presents the mean velocity and turbulence intensity profiles measured at planes 1, 2 and 3 with the Newtonian fluid at a Reynolds number of 8900 and with the 0.2% aqueous solution of CMC at Reynolds numbers of 1150, 6200 and 9600. No velocity measurements were made on plane 4 due to the large deflection of the light

(*a*) Tetraline/turpentine mixture

Bulk Reynolds number		Plane 1	Plane 2	Plane 3	Plane 4	U_{m1}/U_{m3}
8900	U_m (m/s)	0.60	0.92	1.10	0.88	0.54
—	Local *Re*	1950	6400	10100	6500	—
26600	U_m (m/s)	1.83	2.60	3.04	2.52	0.6
—	Local *Re*	6000	18200	28000	18500	—

(*b*) 0.2% Aqueous solution of CMC

Bulk Reynolds number		Plane 1	Plane 2	Plane 3	U_{m1}/U_{m3}
1150	U_m (m/s)	0.46	0.91	1.15	0.40
—	Local *Re*	250	1060	1770	
6200	U_m (m/s)	1.80	2.51	2.64	0.68
—	Local *Re*	1490	4450	6190	
9600	U_m (m/s)	2.60	3.48	3.69	0.70
—	Local *Re*	2400	6900	9700	

TABLE 4. Circumferential variation of maximum velocity

beams but they can be considered to be similar to those of plane 2. The differences in the mean velocities are slightly less than those obtained with the concentric annulus and tend to increase as the distance between the cylinder walls increases. The conclusion drawn from figure 4, that the non-Newtonian fluid had a greater effect than the variation in effective Reynolds number, is no longer evident. The fluctuation velocity profiles are, however, similar to those of figure 4(*b*) and again the polymer tends to suppress fluctuations in the directions normal to that of the bulk flow. A general reduction in the magnitude of the turbulence intensities as the gap between the cylinders is reduced is also apparent, presumably as the Reynolds number based on the gap width is reduced. Table 4 summarizes the maximum velocities of the Newtonian and 0.2% CMC flows at each plane together with the ratio of maximum velocities of plane 1 and 3, and local effective Reynolds numbers based on gap width and the corresponding maximum velocity.

It is evident from table 4 that the difference in maximum velocities for planes 1 and 3 increases with decreasing bulk Reynolds number for both the Newtonian fluid and CMC, with the greatest difference at the lowest effective bulk Reynolds number of 1150 for the 0.2% CMC solution and that, at a similar bulk Reynolds number, the difference between the ratio of the maximum velocities for these fluids is 23%. The results also show considerable circumferential variations of local Reynolds number so that, in some cases, the flow in the narrowest gap approaches transitional values. For example, the Newtonian and 0.2% CMC fluids at bulk Reynolds numbers of 8900 and 9600 have corresponding local Reynolds numbers on the narrow gap of 1950 and 2400 respectively. The turbulence intensity results of figure 9 for the narrowest gap precludes the possibility that the flow is laminar.

The near- outer-wall velocity profiles are shown in wall-law coordinates in figure 10 together with the variation of skin-friction coefficient with Reynolds number. As in figure 5(*a*) for the concentric annulus, the profiles tend to have logarithmic regions which lie between the usual law of the wall and that of the maximum drag reduction asymptote, due to the drag reduction effect, and the deviations from the law of the wall increase as the gap between the walls decreases, due to the reduction in local effective Reynolds number. As before, the polymer tends to reduce the skin-friction coefficient

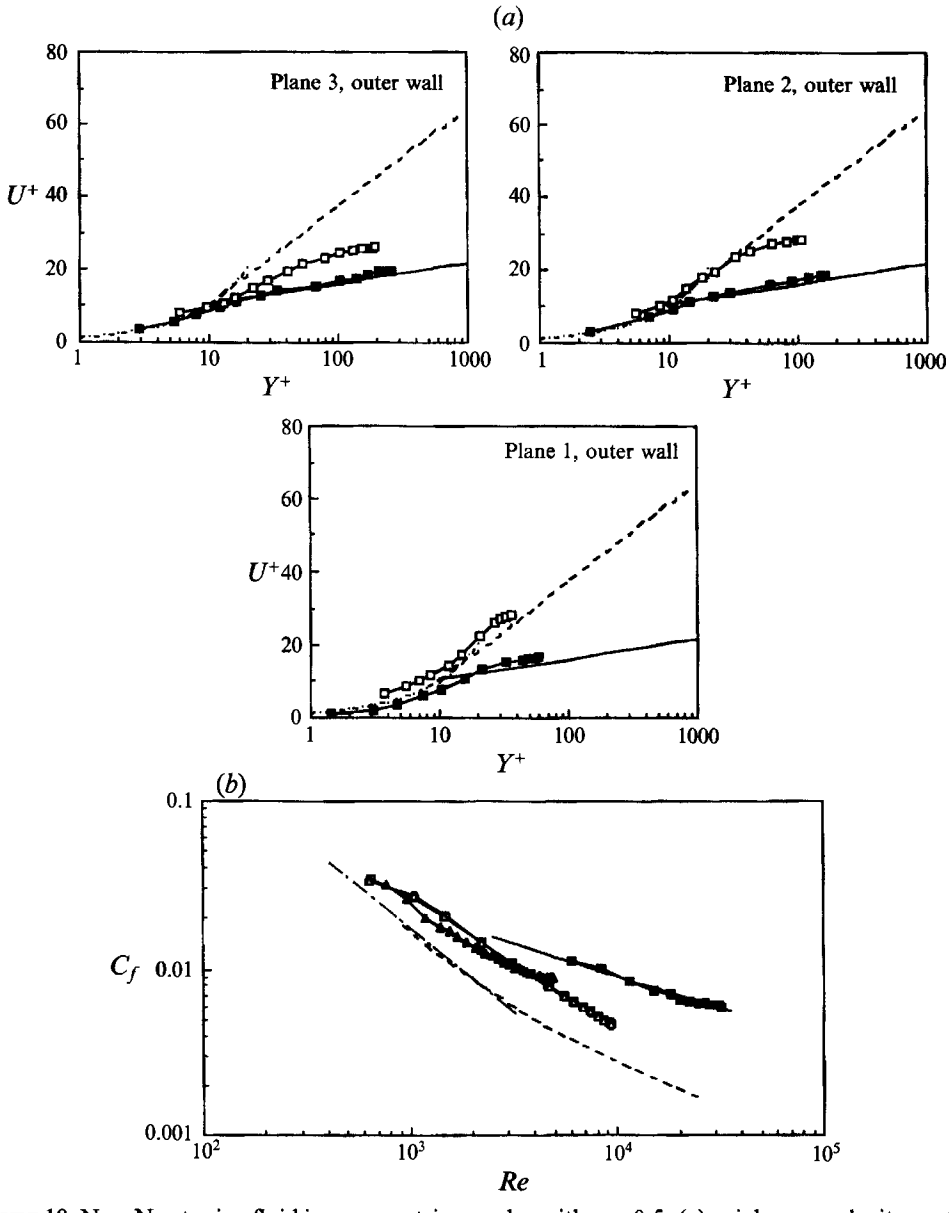

FIGURE 10. Non-Newtonian fluid in an eccentric annulus with $e = 0.5$: (*a*) axial mean velocity profiles in law-of-the-wall coordinates for an effective Reynolds number of 9600, symbols the same as in figure 4 and ——, $U^+ = 2.44 \ln Y^+ + 4.9$; – – – – –, $U^+ = Y^+$; – – –, $U^+ = 11.7 \ln Y^+ - 17$; (*b*) skin-friction coefficient as a function of Reynolds number: ——, $C_f = 0.33 Re^{-0.39}$; – – – – –, $C_f = 17.7 Re^{-1}$; ——, maximum drag-reduction asymptote. For symbols see figure 5.

and this is emphasized by the reduction in the gap between the cylinder walls more than by the effective Reynolds number. The variation of the skin-friction coefficient for the polymer solution with Reynolds number is shown in figure 10(*b*) together with Newtonian results for turbulent and laminar flows. With the Newtonian fluid in the laminar region, and unlike the concentric annulus flow, the C_f values are 15% higher than the analytical solution for the eccentricity of 0.5 ($C_f = 17.7 Re^{-1}$, Shah & London 1978) and this is also so with the polymer solution. The extension of non-turbulent flow

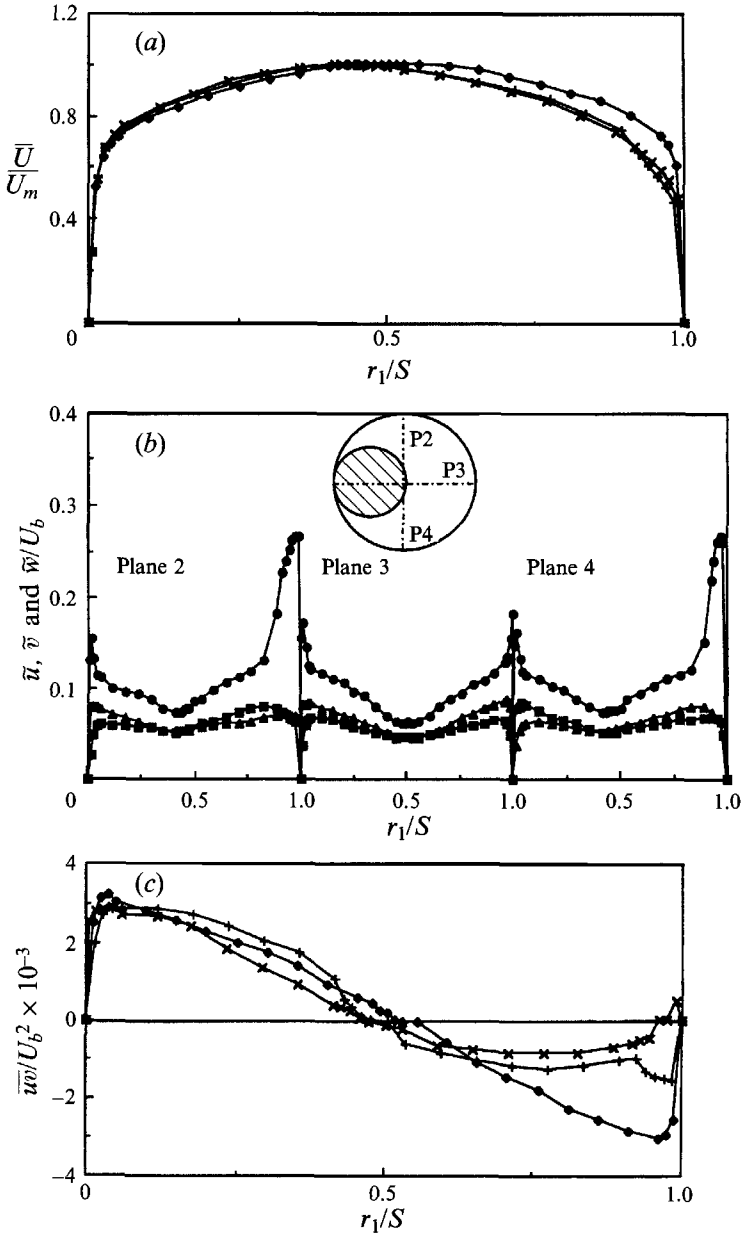

FIGURE 11. Newtonian fluid in an annulus with eccentricity of unity for a Reynolds number of 26600: (*a*) Axial mean velocity, symbols as in figure 6(*a*); (*b*) r.m.s. velocity fluctuations, symbols as in figure 2(*b*); (*c*) $\overline{uv}$ cross-correlation, symbols as in figure 6(*d*).

is evident for the polymer solution, with a drag reduction of about 50% for the highest effective Reynolds number which is about 20% less than that of the concentric flow.

3.2.2. *Eccentricity of unity*

Newtonian turbulent flow at a Reynolds number of 26600 was first investigated with the results shown on figures 11–14. The circumferential variation in the mean velocity profile, figures 11(*a*) and 12(*a*), is considerable with maximum axial velocities in planes 2′, 2, 3, 4 and 4′ corresponding to 0.96, 1.25, 1.42, 1.27 and 1.01 of the bulk velocity,

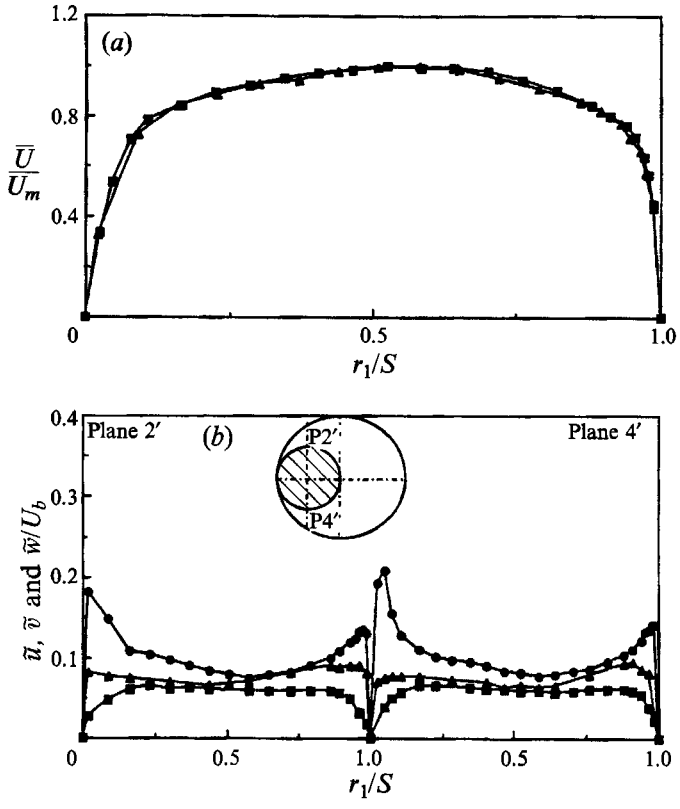

FIGURE 12. Newtonian fluid in an annulus eccentricity of unity for a Reynolds number of 26600: (*a*) axial mean velocity: —■—, plane 2′; —▲—, plane 4′; (*b*) r.m.s. velocity fluctuations, symbols the same as in figure 2(*b*).

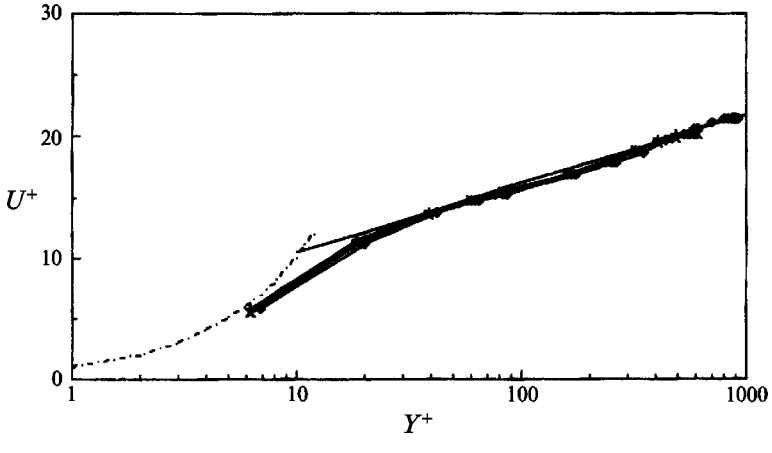

FIGURE 13. Axial mean velocity profiles at the outer wall in law-of-the-wall coordinates: Newtonian fluid in an annulus with eccentricity of unity for a Reynolds number of 26600; ——, $U^+ = 2.44 \ln Y^+ + 4.9$′, – – – – –, $U^+ = Y^+$. For symbols see figure 6(*a*).

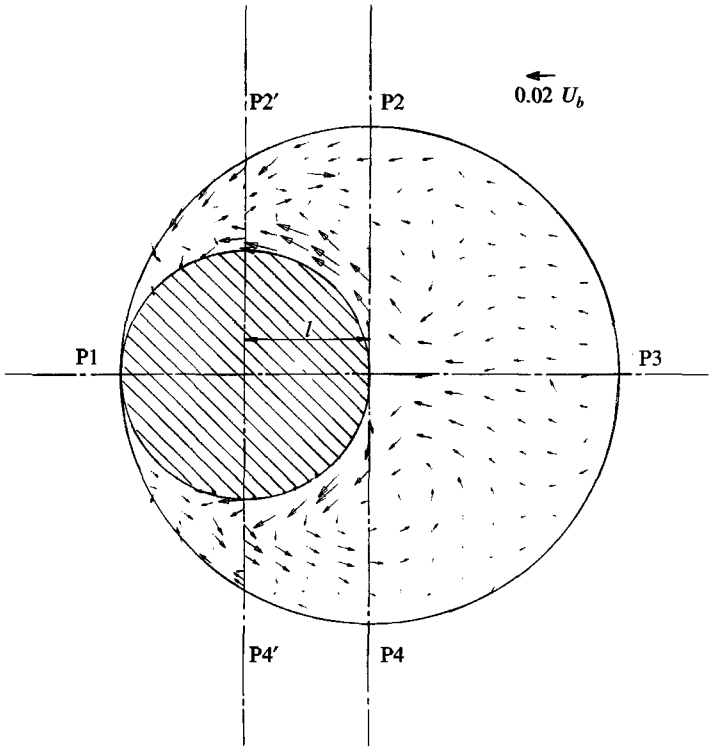

FIGURE 14. Vector velocity distribution of the cross-flow for a Reynolds number of 26600: Newtonian fluid in an annulus with eccentricity of unity.

giving a maximum difference of 32% between planes 2′ and 3 with the locations of maximum velocities close to the centre of the gaps. The differences between the maximum velocities of the symmetrical planes 2′ and 4′, and 2 and 4 are up to 5% for the reason given in the previous section, and the maximum velocity in plane 3 is similar to that for an eccentricity of 0.5. The velocity profiles of planes 2 and 4 are more skewed than that of plane 3, particularly in the region close to the inner wall where there is severe inner wall curvature, and this is reflected in the high axial velocity fluctuations in that region, figure 11(*b*). The velocity fluctuation profiles show similar patterns to those with an eccentricity of 0.5, decreasing from axial, to circumferential to radial components. The shear stress coefficient, $\overline{uv}/U_b^2$, has an extensive linear region close to the outer wall for planes 2, 3 and 4 and close to the inner wall of plane 3. The nonlinearity of the results in planes 2 and 4 in the inner wall region is because these planes are not perpendicular to the inner wall. The locations of zero shear stress are again at the middle of the gaps, within measurement precision.

The mean velocity profiles close to the outer wall are presented in wall-law coordinates in figure 13 and are in good agreement with the law of the wall for planes 2, 3 and 4, as was the case for the eccentricity of 0.5. The variations of skin-friction factors with Reynolds number correspond to a correlation curve of $C_f = 0.28Re^{-0.39}$ over the measured range of Reynolds number. The values of C_f were 22.5 and 16% smaller than those for an eccentricity of zero and 0.5 respectively and in accord with the finding of Jonsson & Sparrow.

Secondary flow vectors were measured with the Bragg-cell method and figure 14 indicates values up to 2.5% of the bulk velocity, which is 35% greater than detected with an eccentricity of 0.5. There are four circulation cells, two on each side of the

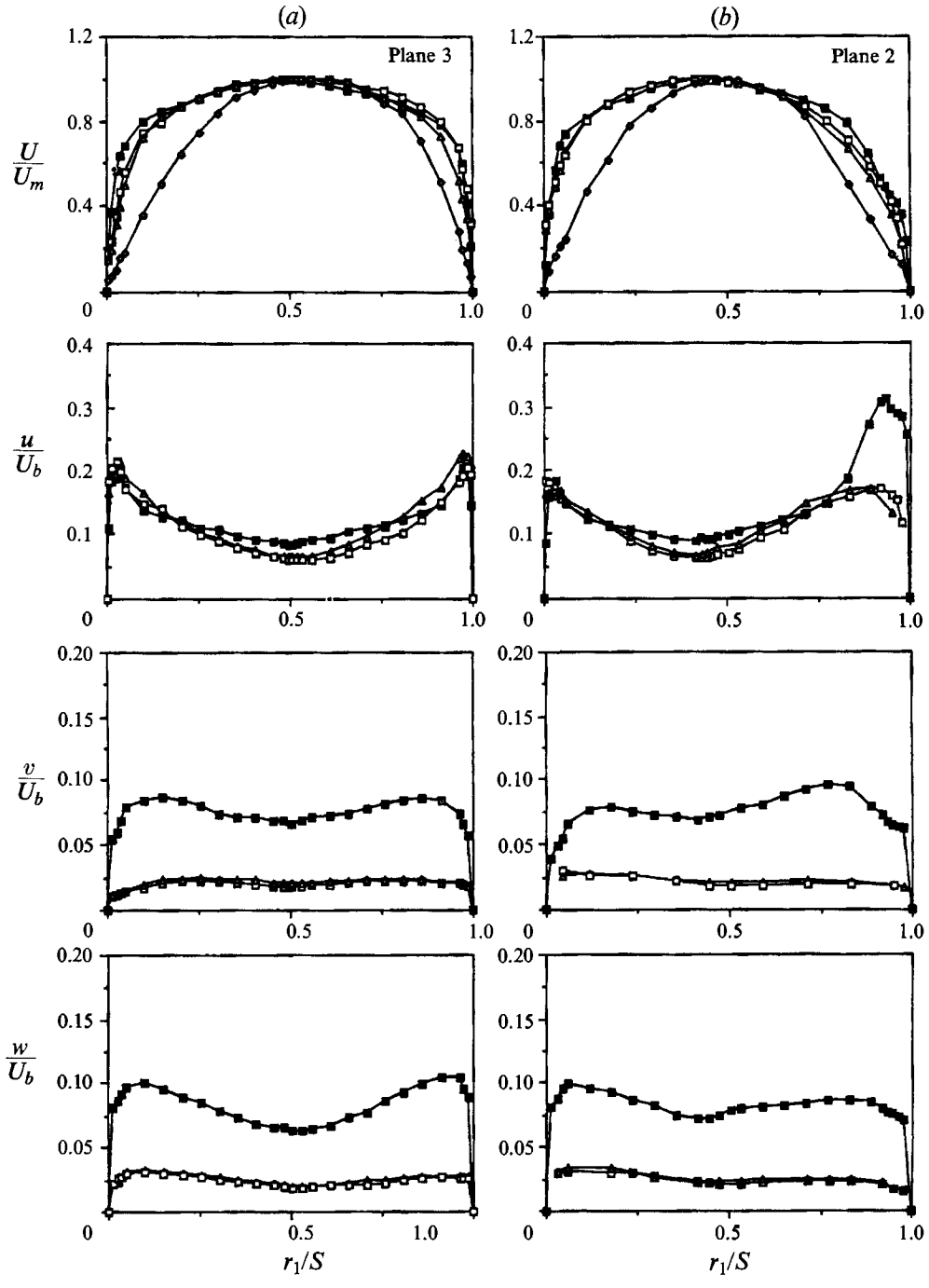

FIGURE 15. Mean and r.m.s. velocities of non-Newtonian fluid in an annulus with eccentricity of unity for three effective Reynolds numbers: (*a*) plane 3; (*b*) plane 2. For symbols see figure 4.

plane of symmetry with the larger pair located close to the inner wall and plane 2–4, and the smaller pair at the narrower gap close to the outer wall and plane 2′–4′. The vectors suggest transport of fluid from wider to narrower regions and that this

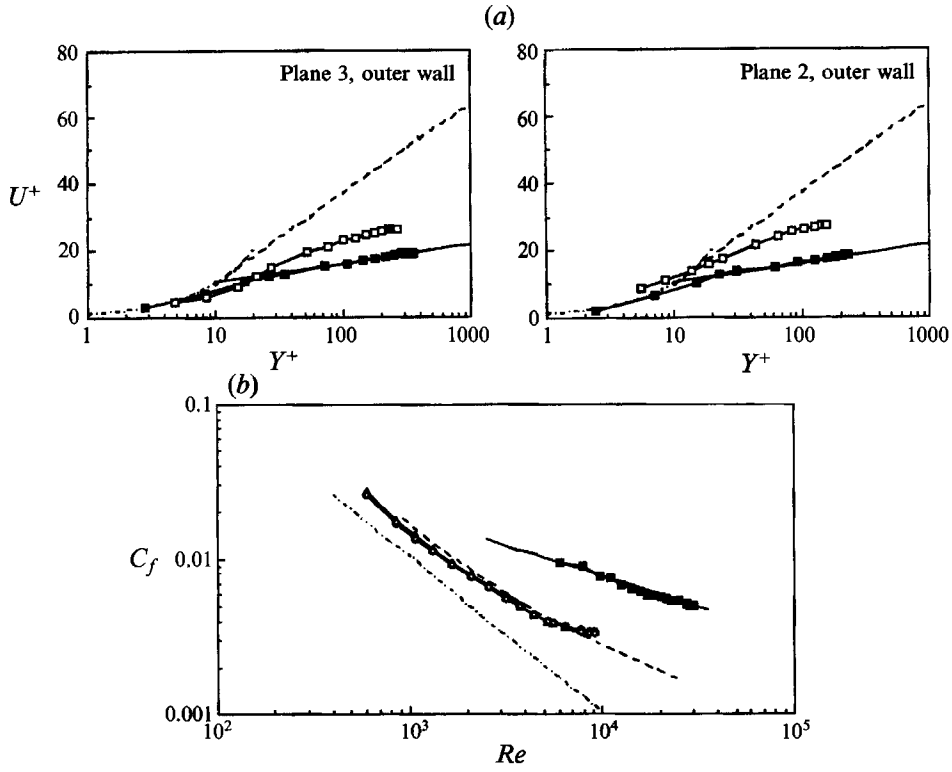

FIGURE 16. Non-Newtonian fluid in an annulus with eccentricity of unity: (*a*) axial mean velocity profiles in law-of-the-wall coordinates for an effective Reynolds number of 9600, symbols the same as in figure 4, and ——, $U^+ = 2.44 \ln Y^+ + 4.9$; – – – – –, $U^+ = Y^+$; – – –, $U^+ = 11.7 \ln Y^+ - 17$. (*b*) skin-friction coefficient as a function of Reynolds number; ——, $C_f = 0.28 Re^{-0.39}$; – – – – –, $C_f = 10.26 Re^{-1}$; – – –, maximum drag-reduction asymptote. For symbols see figure 5.

transport is stronger along the inner pipe wall, which may explain the distortion of the axial velocity profile in that region.

Measurements of velocity and wall pressure were also obtained with the Newtonian fluid at a Reynolds number of 8900 and with the polymer solution at effective Reynolds numbers of 1150, 6200 and 9600. Similar patterns to those for an eccentricity of 0.5 can be seen in figure 15 with almost the same mean velocity profiles for the Newtonian and non-Newtonian fluids at similar Reynolds numbers: with the CMC solution, the mean velocity profiles change with effective Reynolds number so that they have near-wall forms closer to that expected for laminar flow at the lowest effective Reynolds number. The effect of the polymer solution on the fluctuation velocity profiles is similar to those with eccentricities of 0 and 0.5 with considerable suppression of cross-flow fluctuations.

The mean velocity profiles near the outer wall are shown in wall-law coordinates in figure 16 together with the variation of the skin-friction coefficient with Reynolds number. The mean velocity profiles for the polymer solution, figure 16(*a*), tend to have logarithmic regions similar to those with eccentricities of 0 and 0.5 and lie between the Newtonian results, in accord with the expected law of the wall, and that of the maximum drag-reduction asymptote. The deviation from the law of the wall also increases as the gap between the bounding walls reduces and the results again show that the influence of the effective Reynolds number is small compared to that of the reduction of the gap between the cylinders. The variations of friction factor, figure

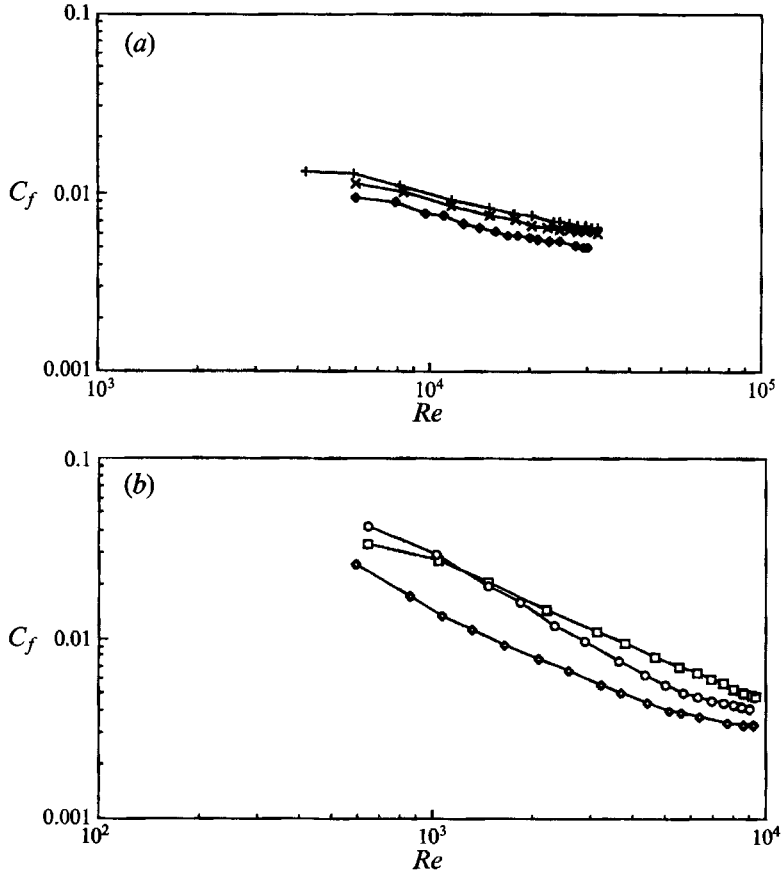

FIGURE 17. Skin-friction coefficient as a function of Reynolds number. (*a*) Newtonian fluid: ——, $e = 0$; —×—, $e = 0.5$; —◆—, $e = 1.0$; (*b*) non-Newtonian fluid: —○—, $e = 0$; —□—, $e = 0.5$; —◇—, $e = 1.0$.

16(*b*), are the same at all orthogonal planes, as was the case for Newtonian fluid flow, with distributions similar to that of maximum drag reduction and, in the laminar region, 22% higher than the Newtonian analytical solution for the eccentricity of unity ($C_f = 10.26Re^{-1}$, Shah & London, 1978). The extension of non-turbulent flow is again evident for the polymer solution, with a drag reduction of about 57% for the highest effective Reynolds number.

The pressure drop do not reduce monotonically with increase in eccentricity, as suggested by Shah & London (1978), and figure 17 allows comparison of the skin-friction coefficients for Newtonian and non-Newtonian fluids for all eccentricities. In turbulent flow of the Newtonian fluid, figure 17(*a*), the results are as expected with C_f higher for an eccentricity of 0 than for 0.5 and 1.0 by 8% and 22.5% respectively. With the polymer solution, figure 17(*b*), this monotonic pattern no longer exists and the values of C_f with zero eccentricity are much higher than with an eccentricity of unity and smaller than with an eccentricity of 0.5, particularly in the region $2000 < Re < 10000$. A possible explanation is that the flow is not fully developed, suggesting a longer hydrodynamic entry length as proposed by Shah & London (1978). The entry length of the present arrangement ($116d_h$) is more than sufficient to produce fully developed laminar flow in a concentric annulus, but it will produce fully developed

laminar flow in the eccentric annulus only for Reynolds numbers below 500. The results for a Reynolds number of 500, figure 17(*b*), show a monotonic reduction of flow resistance, with the concentric annulus values higher than for the two eccentricities, although the uncertainty is around 2.5%.

Drag reduction with polymer solutions is a direct result of the stretching of the molecules in turbulent flow under the action of high strain rate and low vorticity so that the onset requirement for molecular stretching is fulfilled. The mechanism of drag reduction has been investigated by many authors, for example Lumley (1977) and Durst, Haas & Interthal (1982) who explained that the extension of molecules increases the viscosity of the solution in the turbulent region which suppresses the energy-containing eddies in the buffer layer to result in a thickening of the sublayer and a reduction of drag. The indications are a reduction in drag coefficient, suppression of turbulence intensities, and a shift of the turbulent core region to a higher value of Y^+. These features are present in the results of figures 4, 5, 9, 10, 15 and 16 which confirm the delay of transition, with more than threefold suppression of the cross-flow turbulence intensities and, therefore, decrease in drag coefficient when compared to a Newtonian fluid flow at the same Reynolds number. It is evident that the near-outer-wall velocity profiles for the 0.2% CMC solution have logarithmic regions which lie between the usual law of the wall and that of the maximum drag reduction asymptote at higher values of Y^+, with almost the same slope for Newtonian and 0.2% CMC flows, suggesting that the interaction between mean flow and turbulence is unchanged in the core region for both flows.

4. Conclusions

The following statements summarize the more important conclusions which may be drawn.

(i) The results obtained with a Newtonian fluid at a Reynolds number of 26600 are, for the concentric annulus, in accord with expectations and provide evidence of the measurement accuracy. With an eccentricity of 0.5, they show that the maximum axial velocity varied circumferentially from $0.85U_b$ to $1.41U_b$, that the near-outer-wall flow accords with the expected law of the wall except in the narrowest gap and that there was a cross-flow from the wide to the narrow gap with velocities less than around $0.015U_b$. Similar changes of axial flow from narrow to wide gap were evident with an eccentricity of unity, as was a secondary flow with two pairs of circulation each side of the plane of symmetry with velocities less than around $0.025U_b$.

(ii) The variation of skin-friction coefficient of the Newtonian fluid with Reynolds number shows that the flow resistance increased with concentric annulus flow by 8% compared to smooth pipe flow and decreased as the eccentricity increased, so that the flow resistance with an eccentricity of unity is 22.5% less than that with a concentric annulus. With the polymer solution in concentric and eccentric annuli, the skin-friction coefficient varied at the same rate as that of the maximum drag-reduction curve up to the maximum Reynolds number of 9600 with a large extension of non-turbulent flow associated with drag reductions of the order of 63, 50 and 57% for eccentricities of 0, 0.5 and 1.0 respectively.

(iii) The mean velocity results with the 0.2% CMC solution show a similar circumferential variation of the maximum axial velocity to that of the Newtonian fluid in eccentric-annulus flows; the near-outer-wall velocity profiles between the Newtonian profiles and that of the maximum drag-reduction curve have a logarithmic slope in the core region similar to that for the Newtonian fluid.

(iv) The non-Newtonian fluid exhibited values of the r.m.s. axial velocity

fluctuations which decreased slightly with effective Reynolds numbers of 9600, 6200 and 1150 and, at a similar Reynolds number to the Newtonian fluid flow, the axial velocity fluctuations of the polymer solution were slightly suppressed. In all cases, the corresponding fluctuations in the cross-stream direction were suppressed threefold due to the molecular stretching in a manner consistent with previous observations in pipe flow. This was least noticeable in the narrowest gap of the eccentric arrangements due to the low velocities, and corresponding deviations from the logarithmic law of the wall were noted.

Financial support from British Petroleum PLC is gratefully acknowledged. Frequent meetings with Professor M. P. Escudier of the University of Liverpool and Dr C. Lockyear and colleagues at British Petroleum helped greatly in the conduct of the research. We are particularly indebted to Professor Escudier for his careful reading of and comments on this manuscript.

REFERENCES

BRIGHTON, J. A. & JONES, J. B. 1964 Fully developed turbulent flow in annuli. *Trans. ASME* D: *J. Basic Engng* **86**, 835–844.

DURST, F., HAAS, R. & INTERTHAL, W. 1982 Laminar and turbulent flows of dilute polymer solution: a physical model. *Rheo. Acta* **21**, 572–577.

DURST, F., MELLING, A. & WHITELAW, J. H. 1981 *Principles and Practice of Laser-Doppler Anemometry*, 2nd edn. Academic.

JONSSON, V. K. & SPARROW, E. M. 1966 Experimental on turbulent flow phenomena in eccentric annular ducts. *J. Fluid Mech.* **25**, 65–85.

KACKER, S. C. 1973 Some aspects of fully developed turbulent flow in non-circular ducts. *J. Fluid Mech.* **57**, 583–602.

LAWN, C. J. & ELLIOTT, C. J. 1971 Fully developed turbulent flow through concentric annuli. *CEGB Rep.* RD/B/N 1878.

LUMLEY, J. L. 1977 Drag reduction in two phase and polymer flows. *Phys. Fluids* **20**, S64–S71.

MELLING, A. & WHITELAW, J. H. 1976 Turbulent flow in a rectangular duct. *J. Fluid Mech.* **78**, 289–315.

NOURI, J. M. & WHITELAW, J. H. 1991 Particle velocity characteristics of dilute to moderately dense suspension flows in stirred reactors. *Intl J. Multiphase Flow* **18**, 21–33.

NOURI, J. M., WHITELAW, J. H. & YIANNESKIS, M. 1988 A refractive index matching technique for solid/liquid flows. In *Laser Anemometry in Fluid Mechanics* vol. 3, p. 335.

PARK, J. T., MANNHEIMER, R. J., GRIMLEY, T. A. & MARROW, T. B. 1989 Pipe flow measurements of a Transparent non-Newtonian slurry. *Trans. ASME* I: *J. Fluids Engng* **111**, 331–336.

PINHO, F. T. & WHITELAW, J. H. 1990 Flow of non-Newtonian fluids in a pipe. *J. Non-Newtonian Fluid Mech.* **34**, 129–144.

PINHO, F. T. & WHITELAW, J. H. 1991 The flow of non-Newtonian fluids over a confined baffle. *J. Fluid Mech.* **226**, 475–496.

QUARMBY, A. 1967 An experimental study of turbulent flow in concentric annuli. *Intl J. Mech. Sci.* **9**, 205–221.

REHME, K. 1974 Turbulent flow in smooth concentric annuli with small radius ratios. *J. Fluid Mech.* **64**, 263–287.

SHAH, R. K. & LONDON, A. L. 1978 *Laminar flow forced convection in ducts.* Academic.

SMITH, S. L., LAWN, C. J. & HAMLIN, M. J. 1968 The direct measurement of wall shear stress in an annulus. *CEGB Rep* RD/B/N 1232.

SPARROW, E. M., ECKERT, E. R. & MINKOWYCZ, W. J. 1963 Heat transfer and skin friction for turbulent boundary-layer flow longitudinal to a circular cylinder. *Trans. ASME* E: *J. Appl. Mech.* **30**, 37–43.

VIRK, P. S., MICKLEY, H. S. & SMITH, K. A. 1970 The ultimate asymptote and mean flow structure in Toms' phenomenon. *Trans. ASME* E: *J. Appl. Mech.* **92**, 488–493.